Flow-regulated nucleation protrusion theory for collapsed polymers

Sagar Kania,[1] Alparslan Oztekin,[1] Xuanhong Cheng,[2,3] X. Frank Zhang,[3] and Edmund Webb, III[1,*]
[1]*Department of Mechanical Engineering and Mechanics, Lehigh University, Bethlehem, Pennsylvania 18015, USA*
[2]*Department of Material Science and Engineering, Lehigh University, Bethlehem, Pennsylvania 18015, USA*
[3]*Department of Bioengineering, Lehigh University, Bethlehem, Pennsylvania 18015, USA*

(Received 25 May 2021; accepted 28 October 2021; published 22 November 2021)

The globular-stretch transition of a collapsed polymer in low strain rate elongational flow is studied using polymeric protrusion kinetics scaling laws and numerical simulation. Results demonstrate the influence of fluid flow on the occurrence probability of long-length thermally nucleated polymeric protrusions, which regulate collapsed polymer unfolding in low strain rate flows. Further, we estimate that the globular-stretch transition rate (k_s) in low strain rate ($\dot{\epsilon}$) elongational flows varies as $k_s \sim e^{-\alpha\dot{\epsilon}^{-1}}$. Results here reveal that the existing approach of neglecting the effects of fluid flow on thermally nucleated protrusions distribution is not valid for analyzing polymer unfolding behavior in low strain rate flows. Neglecting such an effect overestimates the constant α in the scaling law of transition rate ($k_s \sim e^{-\alpha\dot{\epsilon}^{-1}}$) by a factor of 2.

DOI: 10.1103/PhysRevE.104.054504

I. INTRODUCTION

There is significant interest in understanding the dynamic behavior of collapsed polymer chains in solution, particularly when they are subject to flow conditions [1–3]. One motivation for this is understanding the behavior of self-associated biological macromolecules that exhibit fluid flow-regulated functionality [4–6]. For example, the blood clotting process initiated by the von Willebrand factor (vWF)—a large multimeric glycoprotein—relies upon the hydrodynamic characteristics of collapsed globules in flow [5,6]. The globular-stretch transition behavior of collapsed polymers is quite different from the classical coil-stretch transition [7,8], in which configuration entropy dominates the elastic response of flexible coils [7–11]. Entropic force resisting the coil-stretch transition causes such transition to be a continuous process when extensional force is applied to the polymer ends [12,13]. For collapsed polymers, entropy becomes secondary to monomer-monomer interaction in opposing stretching [13,14]. Further, when a collapsed polymer is stretched at both ends, the restoring force's dependence is initially linear but becomes constant above a relatively low threshold deformation, i.e., after the manifestation of a polymeric strand [7,12–16]. This restoring force versus deformation trend causes the collapsed polymer's stretching transition to be abrupt when an extensional force applied to the polymer ends exceeds the threshold value [8,13,15].

The globular-stretch transition of collapsed polymers in fluid flows is caused by a thermally nucleated protruding chain end [17–20]. When a protrusion gets long enough to be subject to sufficient hydrodynamic force to overcome the globule's restoring force, it gets pulled from the globule surface, thereby unfolding the polymer [17–19,21]. So, to initiate unfolding, a thermally nucleated protrusion requires some minimum length, depending on the flow condition; with the increment of the strain rate, the required protrusion length to unfold decreases [17–19,21]. Since the underlying mechanism for collapsed polymer unfolding is similar to classical nucleation theory, prior authors characterized the strain rate as the critical strain rate at which the minimum protrusion length required to unfold the polymer is equal to the ensemble-averaged length of the thermally nucleated protrusion [17–19,21]. This implies that unfolding occurs effectively instantaneously for a strain rate greater than or equal to the critical value.

A previous investigation by Sing *et al.* has proposed that the protrusions governing the collapsed polymer globular-stretch transition in high strain rate elongational flows (strain rate $\geqslant$ critical strain rate) are much shorter than the remaining globule radius (i.e., short-length protrusions) and that the occurrence of thermally nucleated protrusions is independent of the fluid flow [19,21]. This model accurately estimates the dependence of critical strain rate on the various polymer parameters [19,21]. However, despite identifying the critical strain rate for a given collapsed polymer, the above model may not be valid for studying polymer unfolding behavior across a broad range of strain rates. As for strain rate well below the critical value, the protrusion length required to unfold the polymer is longer than the remaining globular radius [22]. Therefore, their occurrence probability might be flow rate dependent. In the present study, a strain rate for which the required protrusion length to drive unfolding is larger than the remaining globule radius is considered a "low" strain rate. The motivation for understanding the unfolding of collapsed polymer in low strain rate elongation flows comes from our recent study on the vWF protein [23], whose unfolding behavior in the bloodstream can be described by the physics of collapsed polymers in flow [5]. This work suggests that though the probability of vWF protein unfolding in low strain rate flows is significantly lower compared to high strain flows,

*ebw210@lehigh.edu

such an unfolding process can still be associated with clotting anomalies [23]. Moreover, we expect that investigating collapsed polymer unfolding in low strain rate elongational flows could further elucidate other self-associated biological macromolecules conformation-regulated functionality since such macromolecules are frequently subjected to low strain rate flows when they transit through the circulation. Hence, it is crucial to understand the collapsed polymer's unfolding behavior subjected to low strain rate flows, thereby making the kinetic study of thermally nucleated long-length protruding chain ends (i.e., protrusions longer than the remaining globule radius) essential.

We estimate the protrusion length distribution function (PDF) for long-length protrusions for collapsed polymers in uniaxial elongational flow to demonstrate how the fluid flow regulates the occurrence probability of those protrusions. The occurrence of a thermally driven long-length protrusion is negligible for polymers subjected to a strain rate equal to or greater than the critical strain rate. In that strain rate range, a short-length protrusion induces the unfolding of a collapsed polymer [19,21]. Further, our recent study illustrates that the mean first passage time of a collapsed polymer globular-stretch transition in low strain rate flows can extend to tens of minutes or hours, while standard stochastic dynamic simulation trajectories are typically limited to a timescale of seconds [23]. This result indicates that the probability of protrusions initiating such transition (long-length protrusions) is very low over the timescale of standard stochastic dynamic simulation. So, an enhanced sampling technique, Weighted Ensemble, is coupled with Brownian dynamic simulation (i.e., WEBD) to adequately sample states with a thermally driven long-length protrusion, thereby validating our hypothesized PDF for long-length protrusions via numerical results. Moreover, we examine the importance of flow-regulated protrusion distribution for analyzing the unfolding behavior of a collapsed polymer in low strain flows. For such analysis, we derive the scaling laws of globular-stretch transition rate considering the flow-dependent and flow-independent thermally nucleated protrusion distribution and compare them with the simulation results.

II. METHODOLOGY

A. Collapsed polymer model and Brownian dynamics simulation

The motivation of this work comes from our recent study, where we illustrated the importance of understanding the collapsed polymer globular-stretch transition behavior in elongational flows having a strain rate less than the critical value [23]. In particular, in that work, we illustrated that the unfolding of one of the collapsed biopolymers—vWF proteins—in strain rate flows below the critical value can lead to pathology. In this work, we employed a coarse-grained model of collapsed polymers similar to that prior work and it is summarized here. The model represents a collapsed polymer by the well-known bead-spring polymer model [9]. The spherical beads act as discretized sources of friction, the backbone of the polymer chain is realized by a series of springs that connects neighboring beads, and self-association of the polymer is described via interaction between nonadjacent beads. Our bead-spring model is composed of $N = 160$ beads of radius $a = 15$ nm interacting through a potential $U = U_s + U_{LJ}$. U_s which accounts for the connectivity of the chain is given as $U_s = \frac{k}{2}\sum_{i=1}^{N-1}(r_{i+1,i} - r_{eq})^2$, where $r_{i+1,i}$ is the distance between adjacent beads. The spring constant is taken to be $k = 200k_bT/a^2$, which limits the bead-spring polymer model to stretch beyond its contour length to a negligible level [17,19,24]. Spring equilibrium length is considered as $r_{eq} = 2.07a$ (∼31 nm). The Lennard-Jones potential represents the self-association of the polymer $U_{LJ} = u\sum_{ij}[(r_{eq}/r_{ij})^{12} - 2(r_{eq}/r_{ij})^6]$, where r_{ij} is the distance between the ith and jth bead and u determines the depth of the potential. To model a collapsed polymer, u is considered as $1.0k_bT$ [17].

For Brownian dynamics (BD) simulation, the dynamics of the ith bead position $\mathbf{r}_i$ is given by the overdamped Langevin equation [25]:

$$\mathbf{r}_i^{t+\Delta t} = \mathbf{r}_i^t + \left[\mathbf{v}_\infty(\mathbf{r}_i^t) - \frac{1}{k_bT}\sum_{j=1}^{N}\underline{D}_{ij}\left(\mathbf{r}_i^t, \mathbf{r}_j^t\right).\nabla_{\mathbf{r}_j^t}U(t)\right]\Delta t + \mathbf{R}_i(\Delta t), \tag{1}$$

where $\mathbf{r}_i^t$ and $\mathbf{r}_i^{t+\Delta t}$ are the position of the ith bead at time step t and $t + \Delta t$, respectively. $\mathbf{v}_\infty(\mathbf{r})$ is the undisturbed solvent flow profile and $\mathbf{R}_i(\Delta t)$ is a random displacement whose average is 0 and variance-covariance is $\langle\mathbf{R}_i(\Delta t)\mathbf{R}_j(\Delta t)\rangle = 2\underline{D}_{ij}\Delta t$. For uniaxial elongational flow, the undisturbed flow profile is $\mathbf{v}_\infty(\mathbf{r}) = \dot{\epsilon}[x\hat{\mathbf{x}} - 0.5y\hat{\mathbf{y}} - 0.5z\hat{\mathbf{z}}]$, where $\dot{\epsilon}$ is the strain rate. x, y, z are the coordinates, and $\hat{\mathbf{x}}$, $\hat{\mathbf{y}}$, $\hat{\mathbf{z}}$ are the unit vectors [19]. Hydrodynamic interaction among beads are manifested in $\underline{D}_{ij}$(diffusion tensor), which is given by the Rotne-Prager-Yamakawa approximation [25–27]:

$$\underline{D}_{ij} = \frac{k_bT}{6\pi\eta a}\underline{\mathbb{I}}; \quad i = j, \tag{2}$$

$$\underline{D}_{ij} = \frac{k_bT}{8\pi\eta r_{ij}}\begin{cases}\left(1 + \frac{2a^2}{3r_{ij}^2}\right)\underline{\mathbb{I}} + \left(1 - \frac{2a^2}{r_{ij}^2}\right)\frac{\mathbf{r}_{ij}\mathbf{r}_{ij}}{r_{ij}^2} & r_{ij} \geqslant 2a \\ \frac{r_{ij}}{2a}\left[\left(\frac{8}{3} - \frac{3r_{ij}}{4a}\right)\underline{\mathbb{I}} + \frac{r_{ij}}{4a}\frac{\mathbf{r}_{ij}\mathbf{r}_{ij}}{r_{ij}^2}\right] & r_{ij} < 2a\end{cases}; \quad i \neq j, \tag{3}$$

where i, j denote beads, $\mathbf{r}_{ij} = \mathbf{r}_j - \mathbf{r}_i$, $\underline{\mathbb{I}}$ is the identity matrix, a is the bead radius, and η is the solvent viscosity. We used solvent (water) viscosity as $\eta = 0.001$ Ns/m^2, and the temperature is $T = 300$ K. Dimensionless variables are designated with a tilde; lengths are normalized by bead radius a, energies by the thermal energy k_bT, and time by the single-bead diffusion time $t_D = 6\pi\eta a^3/k_bT$.

B. WEBD simulation

The WEBD simulation details for collapsed polymers subjected to elongational flows are discussed in a separate paper [23] and summarized here. For the WEBD simulation, similar to prior works, the configuration space is divided into bins along the progress coordinate of the transition event being studied [28–30]. For the study of polymer globular-stretch transition, the progress coordinate is chosen to be the polymer extension in the flow direction. Further, the first and the last bin at each end of the progress coordinate are designated based on the average extension of globular polymer and stretched polymer, respectively. The first bin is identified as the initial state and the last bin as the target state. The number of bins and their placement between the first and last bin is computed based on Kim and Huber's bin placement scheme [23,28].

WEBD simulations are initiated with M noninteracting polymer chains. Initialization of the simulation also requires assigning a probability to each polymer chain as an initial condition for subsequent resampling steps [28,31]. Since the WEBD simulation solution at a steady state is independent of the initial condition, we make a simple choice for initializing the simulation [28,31–33]. All M noninteracting polymer chains were initiated in the first bin (i.e., globule conformation), each assigned a probability $(1/M)$. These polymer chains undergo BD simulation for a fixed time interval ($\tau = 10\,000$ BD steps). After that, polymer chains' extension in flow direction is examined to determine the occupied bins. They are then replicated or deleted as needed so that each occupied bin contains the predetermined number of chains (M). During this resampling step, the probability associated with each polymer chain is reassigned to maintain constant probability within a bin, which naturally conserves total probability across bins (see Ref. [28] for details). After this resampling step, all polymer chains are simulated for another τ time interval, after which the resampling step is again repeated. The whole process of simulating the samples via BD simulation for τ time interval and the resampling step is repeated until the WEBD simulation reaches a steady state. In WEBD simulation, maintaining the predetermined number of polymer chains per occupied bin ensures that the computing resources during the simulation are used uniformly over the entire configuration space independently of the free-energy landscape, and reassignment of polymer chains' probability at the end of resampling step warrants that no bias is introduced in the system's evolution because of resampling.

For the present study, the predetermined number of polymer chains per occupied bin was selected to be $M = 20$. The choice of $M = 20$ polymer chains per occupied bin was arrived at based on a balance between the computational cost of increasing the number of simulations for a given ensemble and the benefit of reducing the statistical variation of each bin's occupational probability. Utilizing more polymer chains per bin will reduce the bins' occupational probability fluctuations and the amount of time each simulation must be run to obtain a reasonably low statistical error; however, increasing the number of independent simulations that must be executed increases parallel computing requirements. We found that 20 samples per bin with sufficient averaging after reaching steady state established a good balance.

A particular criterion is set for a polymer chain entering the target state: throughout the simulation, when any polymer chain enters the target state, its probability is fed back into the initial state by evenly dividing it among samples in that bin. This criterion for polymer chains that reach the target state (i.e., Hill's relation) permits us to directly obtain the globular-stretch transition rate from the probability flux into the last bin [28,33,34]. Kinetics data presented below are computed after WEBD simulations reach a steady-state condition where the probability in each bin and probability flux into the target state oscillate around a well-defined average for that state. For a steady-state WEBD simulation, averaged target-state probability flux equals initial to target state (i.e., globular-stretch) transition rate.

III. RESULTS AND DISCUSSION

A. PDF

In prior studies of collapsed polymers in fluid flow, it was shown that when a polymeric protrusion becomes longer than the critical protrusion length, on average, it will induce unfolding of a collapsed polymer [18,19,21]; critical protrusion length is the minimum length of protrusion required to make hydrodynamic drag force on the protrusion equivalent to the globule's restoring cohesive force. Thus, a polymer having a protrusion length less than or equal to critical protrusion length can be considered to be in a globular state. For a globular-state polymer, though the hydrodynamic drag force on a protrusion is less than the restoring force on the protrusion, the protrusion can still elongate because of thermal bombardment of surrounding fluid on the protruding segment [18,19,21]. Figure 1 illustrates a globular-stretch transition observed in BD simulations of elongation flow presented here; also shown are examples of thermally excited protrusions from a globular-state polymer. The strain rate $\tilde{\epsilon} = 0.061$ shown in Fig. 1 is less than the critical strain rate ($\tilde{\epsilon}^* = 0.095$), computed in a prior work [19]. However, $\tilde{\epsilon} = 0.061$ is still sufficiently high to occasionally observe nucleation of a long enough protrusion to drive conformation transition during a standard BD simulation. When a protrusion nucleates that is sufficiently long (i.e., protrusion having length > critical protrusion length) to drive unfolding, the hydrodynamic drag force acting on the protrusion drives further elongation, leading to a rapid conformation transition; after a conformational change in elongational flow, a polymer remains in a stretch state unless flow is ceased. Figure 1 demonstrates the typical conformations seen during unfolding; as observed previously [19], a thermally nucleated protruding chain end inducing the globular-stretch transition substantially limits the dynamic pathway through which collapsed polymer globule extends, resulting in only half-dumbbell conformations.

Since when a collapsed polymer is in a globular state, protrusions are thermally driven, the protrusion length distribution function follows the Boltzmann distribution. Therefore, the PDF for a globular-state polymer can be given as $P(\tilde{l}) \sim e^{-\emptyset(\tilde{l},\tilde{\epsilon})}$, where $\emptyset(\tilde{l},\tilde{\epsilon})$ is the free energy of globular-state polymer having protrusion of length $(\tilde{l})$ in the elongational

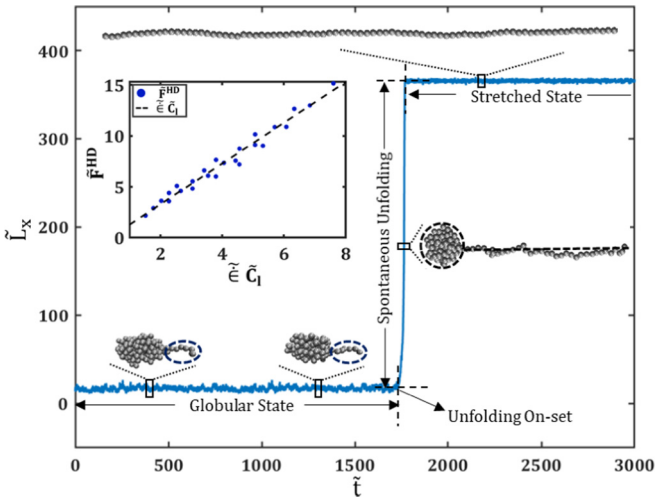

FIG. 1. Plot of polymer extension ($\tilde{L}_x$) in the flow direction as a function of time from BD simulation at the elongational rate $\tilde{\dot{\epsilon}} = 0.061$. The arrows indicate the time duration for which collapsed polymer is in a globular state and the time of spontaneous unfolding. The small rectangles in the various states (globular, spontaneous unfolding, stretched) denote the taken snapshots. Blue dotted lines indicate a thermally driven polymeric protrusion of globular-state polymer. The black dotted lines illustrate collapsed polymer assuming a half-dumbbell configuration during the unfolding process. The inset figure illustrates the hydrodynamic force $\tilde{F}^{HD}$ exerted on the unfolded polymer for varied contour length polymer ($\widetilde{C}_l$) at different elongational rates ($\tilde{\dot{\epsilon}}$). The dashed line represents the scaling law for $\tilde{F}^{HD}$.

flow of strain rate $\tilde{\dot{\epsilon}}$ [20,21]. The free energy of globular-state polymer $[\emptyset(\tilde{l}, \tilde{\dot{\epsilon}})]$ will be the summation of free energy of polymer in no-flow condition $[\emptyset(\tilde{l}, 0)]$ and additional energy $[w^{HD}(\tilde{l}, \tilde{\dot{\epsilon}})]$, which is the contribution from the hydrodynamic drag force of the fluid flow. We assume that $w^{HD} \sim -\tilde{F}^{HD}\tilde{l}$, where $\tilde{F}^{HD}$ is the hydrodynamic force on a protrusion of length ($\tilde{l}$), which is in the opposite direction of the globule's cohesive force exerted on the protrusion.

$$\emptyset(\tilde{l}, \tilde{\dot{\epsilon}}) = \emptyset(\tilde{l}, 0) + w^{HD}(\tilde{l}, \tilde{\dot{\epsilon}}). \tag{4}$$

The free energy of a polymer having a long-length protrusion in a no-flow condition can be given as $\emptyset(\tilde{l}, 0) = k_1\tilde{l}^1$. This is because, for collapsed polymers, the restoring force ($\tilde{F}_{coh} = k_1$) is independent of the protrusion length for protruding chain end longer than the remaining globule radius [7,13,14]. To estimate the scaling law of w^{HD} for a polymer with a long-length protrusion, we neglect the hydrodynamic interaction of the remaining globule. We base this assumption on the observations of Sing *et al.*, who estimated the average flow profile surrounding a collapsed polymer globule in an elongational flow [19]. Their work showed that the globule's effect on the fluid flow field is manifested only in the globule surrounding region of width less than the globule radius, which verifies our above assumption. Further, because of the uniaxial elongational flow field, the monomers in the long-length polymeric strand—on average—can be considered to be aligned (i.e., in the flow direction) similar to that of the unraveled polymer. Hence the scaling relation of $\tilde{F}^{HD}$ with $\tilde{l}$ and $\tilde{\dot{\epsilon}}$ will be similar to the functional relation of hydrodynamic drag force on an unraveled polymer with contour length ($\widetilde{C}_l$) in an elongational flow field of strain rate ($\tilde{\dot{\epsilon}}$).

Hydrodynamic drag force along the entire polymeric protrusion contour is in one direction (i.e., flow direction). However, for freely flowing unraveled polymer in bulk elongational flow, drag force changes its direction at the unraveled polymer's midpoint. Thus, drag force along the freely flowing unraveled polymer in the steady state is not unidirectional. So, to accurately compute the scaling relation of $\tilde{F}^{HD}$ with $\tilde{l}$ and $\tilde{\dot{\epsilon}}$ by utilizing the hydrodynamic force field of unraveled polymer, we perform BD simulation of immobilized unraveled bead-spring polymer rather than free-flowing unraveled polymer in the bulk elongational flow. In BD simulation, unraveled bead-spring polymer is immobilized by fixing its first bead at the origin (i.e., the elongational flow's stagnation point). Fixing the first bead of the unraveled bead-spring polymer at the origin ensures that the hydrodynamic force along the entire unraveled polymer is in one direction (i.e., flow direction) similar to that of the polymeric protrusion. BD simulation data for unraveled bead-spring polymers of varied contour length in different strain rates indicate that the average hydrodynamic force acting on the unraveled polymer is directly proportional to the product of contour length and the strain rate (shown in Fig. 1): $\tilde{F}^{HD} \sim \widetilde{C}_l\tilde{\dot{\epsilon}} \sim \tilde{l}\tilde{\dot{\epsilon}}$.

For the polymer with a long protrusion length, potential energy induced by the fluid flow scales as $w^{HD} \sim -\tilde{\dot{\epsilon}}\tilde{l}^2$. The scaling law of the free energy of a long protrusion in elongational flow is thus $\emptyset(\tilde{l}, \tilde{\dot{\epsilon}}) = k_1\tilde{l} - k_2\tilde{\dot{\epsilon}}\tilde{l}^2$, which gives a representation of the PDF for a globular-state polymer as

$$P(\tilde{l}, \tilde{\dot{\epsilon}}) \sim e^{-k_1\tilde{l}+k_2\tilde{\dot{\epsilon}}\tilde{l}^2}, \tag{5}$$

where k_1 and k_2 are the constants independent of the protrusion length and the strain rate. Since the scaling law of energy is estimated for long-length protrusion, the above PDF is valid for the protrusion longer than the remaining globule radius.

B. Validation of PDF

To validate the hypothesized PDF for globular-state polymers, we perform WEBD simulations of collapsed polymers subjected to an elongational flow of low strain rate ($\tilde{\dot{\epsilon}} = 0.03-0.06$). Since validation requires identifying a polymer chain from the simulation data as being in the globular state (i.e., having protrusion length less than or equal to critical protrusion length), we estimate the critical protrusion length for elongation rates examined here. To compute critical protrusion length, we sort polymer chains at many different times during a simulation according to the number of beads (N_p) present in each of their protrusions. Over the subsequent 10 000 BD steps, it is determined if each protrusion got longer or shorter (i.e., increased or decreased the number of beads in the protrusion). For each extensional flow rate, the number of beads required in the protrusion (N_p^*) is determined for which the protrusion's probability of getting longer becomes equivalent to the protrusion's probability of getting shorter. To convert to critical protrusion length $\tilde{l}^*$, N_p^* is multiplied by the harmonic spring equilibrium length ($\tilde{r}_{eq}$), and results for

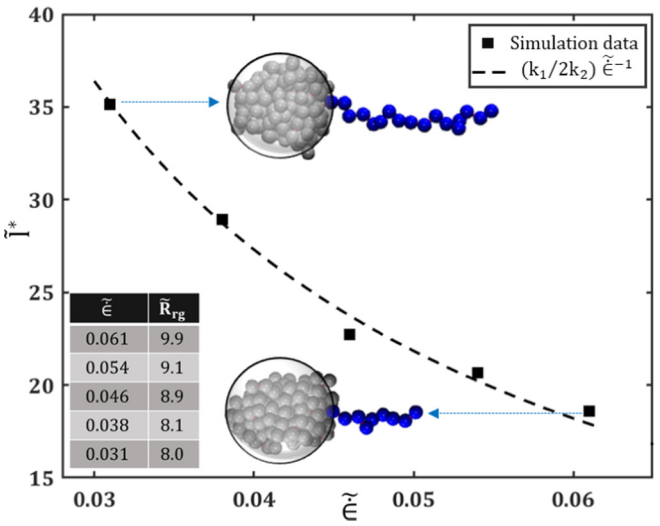

FIG. 2. Critical protrusion length ($\tilde{l}^*$) vs the strain rate ($\tilde{\dot{\epsilon}}$). The dashed line is the derived result Eq. (6), with $k_1 = 1.09$ and $k_2 = 0.50$. Symbols represent the critical protrusion length obtained from WEBD simulations. Snapshot from simulations of polymers exhibiting critical protrusions for $\tilde{\dot{\epsilon}} = 0.061$ and 0.031. Beads in protrusion are colored blue and the circle indicates the remaining globule. The inset table shows the average remaining globule radius ($\tilde{R}_{rg}$) for states with critical protrusion length.

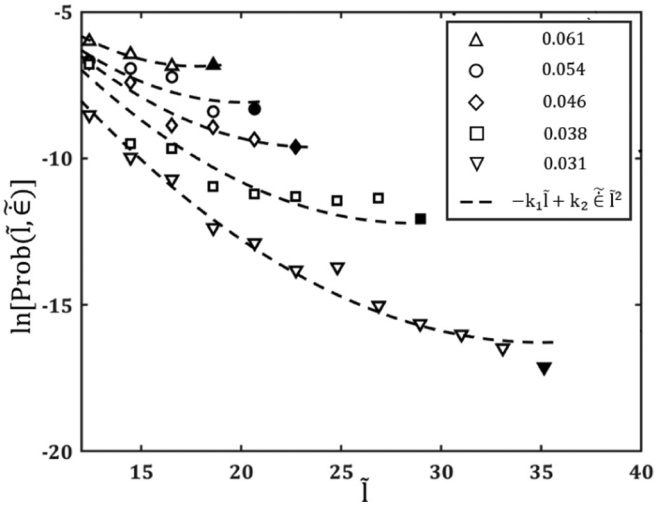

FIG. 3. Occurrence probability of a protrusion from a globular-state polymer as a protrusion length function. The dashed line is the theoretical result Eq. (5), with $k_1 = 1.09$ and $k_2 = 0.50$. Symbols represent the occurrence probability obtained from WEBD simulations, and the filled symbol indicates the critical protrusion length for all elongational rates.

all strain rate flows explored here are shown with symbols in Fig 2.

To further elucidate the dependence of the minimum protrusion length required to unfold the polymer on the low strain rate flows, we derived the functional relation of critical protrusion length with the strain rate, employing long-length protrusions kinetic scaling laws. The restoring force for the collapsed polymer with a long-length protrusion is independent of the protrusion length ($\tilde{F}_{\mathrm{coh}} = \partial[\emptyset(\tilde{l}, 0)]/\partial\tilde{l} = k_1$), and the hydrodynamic force on the long-length protrusion is given as $\tilde{F}^{\mathrm{HD}} = \partial[w^{\mathrm{HD}}(\tilde{l}, \tilde{\dot{\epsilon}})]/\partial\tilde{l} = 2k_2\tilde{l}\tilde{\dot{\epsilon}}$. For $\tilde{F}^{\mathrm{HD}}$ scaling law, the constant is considered $2k_2$ to be consistent with the constant utilized for w^{HD} while deriving the protrusion length distribution function [i.e., Eq. (5)]. When protrusion length becomes equal to critical protrusion length, $\tilde{F}^{\mathrm{HD}} = \tilde{F}_{\mathrm{coh}}$; thus, the critical protrusion length at low strain rate flows can be written as

$$\tilde{l}^* = (k_1/2k_2)\tilde{\dot{\epsilon}}^{-1}. \tag{6}$$

To plot predicted results from Eq. (6), the constants $k_1 = 1.09$ and $k_2 = 0.50$ are required; they are obtained by fitting the simulation data of the protrusion length distribution function [i.e., $P_{\mathrm{sim}}(\tilde{l}, \tilde{\dot{\epsilon}})$] with Eq. (5); this is discussed further below. Using those values, Fig. 2 compares the predicted results for critical protrusion length obtained from Eq. (6) to results obtained from WEBD simulations using the methodology described above, illustrating good agreement between theory and simulation. In addition, for states having protrusion length equal to the critical length, we also computed the radius of the remaining globule. Snapshots from simulations of polymers exhibiting critical length protrusions for $\tilde{\dot{\epsilon}} = 0.061$ and 0.031 are shown in Fig. 2. The inset table in Fig. 2 illustrates that, for the collapsed polymer system studied here, the critical protrusion length is greater than the average remaining globular radius ($\tilde{R}_{rg}$) for all strain rates studied. This verifies that all strain rates studied here are low. It is important to note that the strain rate below which elongational flows can be considered low strain rate flows as defined here will vary for different collapsed polymers. This is because, for a given strain rate flow, the minimum protrusion length required to unfold depends on the polymer size and self-association interaction [19].

Steady-state WEBD simulations predict probability distribution along the progress coordinate, which is polymer extension in the flow direction. For any given bin, its probability represents the probability of that bin's conformation's existence at a given strain rate [35]; here, since extension in the flow direction is directly proportional to protrusion length, that effectively represents the probability of a protrusion length associated with that bin. Thus, we employ those probability values to compute the PDF for a globular-state polymer [i.e., $P_{\mathrm{sim}}(\tilde{l}, \tilde{\dot{\epsilon}})$]. To compute $P_{\mathrm{sim}}(\tilde{l}, \tilde{\dot{\epsilon}})$, we use each polymer chain's probability and corresponding protrusion length at every τ increment during the WEBD simulation. From those data $P_{\mathrm{sim}}(\tilde{l}, \tilde{\dot{\epsilon}})$ is calculated using Eq. (7) below and the results obtained are illustrated in Fig. 3.

$$P_{\mathrm{sim}}(\tilde{l}, \tilde{\dot{\epsilon}}) = \frac{\text{Sum of probability of all polymer chains having protrusion of length } (\tilde{l})}{\text{Sum of probability of all polymer chains having protrusion of length } \tilde{l} \leqslant \tilde{l}^*}. \tag{7}$$

Simulation data in Fig. 3 indicate that the fluid flow significantly alters the occurrence probability of long-length protrusions. To estimate constants of Eq. (5) for the collapsed polymer system studied here, Eq. (5) is fitted to the $P_{\text{sim}}(\tilde{l}, \tilde{\dot{\epsilon}})$ for varied elongational rates with the same k_1 and k_2 since those constants in the proposed PDF are independent of the strain rate. k_1 and k_2 for the best fit are 1.09 and 0.50, respectively. Figure 3 illustrates that Eq. (5) with best-fit constants is in good agreement with the $P_{\text{sim}}(\tilde{l}, \tilde{\dot{\epsilon}})$, verifying the proposed protrusion length distribution function. Figure 3 also indicates that when a point on the curve representing Eq. (5) with $k_1 = 1.09$ and $k_2 = 0.50$ approaches the critical protrusion length, the slope of the curve approaches zero. This is because when protrusion length becomes comparable to critical protrusion length, hydrodynamic drag force ($\tilde{F}^{\text{HD}} = \partial[w^{\text{HD}}(\tilde{l}, \tilde{\dot{\epsilon}})]/\partial\tilde{l}$) acting on it becomes equivalent to the globule restoring force ($\tilde{F}_{\text{coh}} = \partial[\emptyset(\tilde{l}, 0)]/\partial\tilde{l}$).

Though the hypothesized protrusion length distribution function for long-length protrusion is validated for the specific collapsed polymer ($u = 1.0k_bT$ and $N = 160$), it is also valid for a collapsed polymer having different model parameters since the functional form of forces (globule's cohesive force and hydrodynamic force) dictating the probability distribution for long-length protrusions remains the same [12,19]. Nonetheless, constants (k_1 and k_2) of Eq. (5) will vary for different collapsed polymers. For instance, restoring force on the long-length protrusion remains independent of the protrusion length for collapsed polymers in general; however, the value of that force (i.e., $\tilde{F}_{\text{coh}} = k_1$) increases with the increment of N or u [12].

C. Importance of flow-regulated PDF

To elucidate the importance of the flow-regulated thermally nucleated protrusion distribution for analyzing collapsed polymer unfolding behavior under low strain rate elongational flows, we derive the scaling laws of globular-stretch transition rate considering the flow-dependent and flow-independent protrusion distribution.

First, we derive the scaling law for the globular-stretch transition rate considering that the influence of fluid flow on the thermally nucleated protrusions distribution is negligible, which is the general notion employed in prior studies of collapsed polymer unfolding behavior [17–19,21]. So, in this theory, strain rate can only influence the minimum protrusion length required to unfold the polymer, whereas it cannot vary the protrusion distribution [17–19,21]. Therefore, according to this general theory, protrusion length distribution function for long-length protrusion can be given as

$$P(\tilde{l}) \sim e^{-k_1\tilde{l}}, \tag{8}$$

where k_1 is the restoring force for the collapsed polymer with a long-length protrusion. Further, since the globular-stretch transition rate of collapsed polymer in the flow field is proportional to the prevalence of states with the critical protrusion length, Eq. (8) (i.e., flow-independent protrusion distribution) and the functional relation of the critical protrusion length $\tilde{l}^* = (k_1/2k_2)\tilde{\dot{\epsilon}}^{-1}$ [i.e., Eq. (6)] combine to yield the scaling law of globular-stretch transition rate (k_s) with the low strain rate ($\tilde{\dot{\epsilon}}$) as $k_s \sim e^{-\frac{k_1^2}{2k_2}\tilde{\dot{\epsilon}}^{-1}}$.

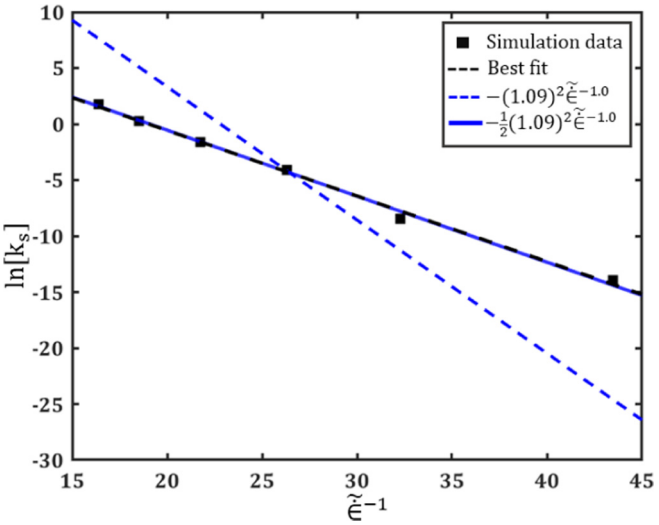

FIG. 4. Globular-stretch transition rate as a function of strain rate. The blue dashed line represents the predicted scaling law $k_s \sim e^{-(1.09)^2\tilde{\dot{\epsilon}}^{-1}}$ and the solid line denotes $k_s \sim e^{-\frac{1}{2}(1.09)^2\tilde{\dot{\epsilon}}^{-1}}$. Square symbols are rates obtained from WEBD simulations, and the black dashed line is the best fit for the simulation data.

In contrast to the general theory, the present study proposed theory states that for analyzing collapsed polymer response in low strain rate flows, it is essential to consider the influence of strain rate not only for critical protrusion length but also for protrusion distribution. When the flow-regulated protrusion distribution [i.e., Eq. (5)] is considered, the scaling law of globular-stretch transition rate is $k_s \sim e^{-\frac{k_1^2}{4k_2}\tilde{\dot{\epsilon}}^{-1}}$. For both cases (i.e., flow-dependent and independent protrusion distribution), transition rate scales as $k_s \sim e^{-\alpha\tilde{\dot{\epsilon}}^{-1}}$. However, when fluid flow influence is neglected for the thermally nucleated protrusion probability distribution, the constant α is overestimated by a factor of 2. To validate this, we estimate the scaling laws of transition rate for the collapsed polymer system studied here, and both scaling laws are fitted to the simulation data, shown in Fig. 4. Constant k_1 and k_2 required to derive the transition rate scaling laws are obtained from Fig. 3.

The scaling law of transition rate is $k_s \sim e^{-\frac{1}{2}(1.09)^2\tilde{\dot{\epsilon}}^{-1}}$ when the flow-dependent protrusion distribution is considered, while for flow-independent protrusion distribution, the transition rate scales $k_s \sim e^{-(1.09)^2\tilde{\dot{\epsilon}}^{-1}}$. Simulation data in Fig. 4 illustrate that k_s varies as $k_s \sim e^{-\alpha\tilde{\dot{\epsilon}}^{-1}}$. The $\alpha = 0.58$ is for best fit to simulation data, in good agreement with the scaling law of k_s, obtained considering the flow-dependent protrusion distribution. Further, the simulation result verifies that neglecting the fluid flow influence on protrusion distribution overestimates the α for the scaling law $k_s \sim e^{-\alpha\tilde{\dot{\epsilon}}^{-1}}$ approximately by a factor of 2. Since the scaling law is valid for any values of k_1 and k_2 (which vary for different collapsed polymers), the result can be extended to collapsed polymers with different parameters. Results here indicate that the influence of fluid flow on protrusion distribution considerably

alters the collapsed polymer's globular-stretch transition behavior in low strain rate flows. Hence, the general notion of neglecting such influence is not valid for analyzing collapsed polymer response under low strain rate flows [17–19,21].

IV. CONCLUSIONS

In summary, we have derived the protrusion length distribution function for thermally nucleated long-length protrusions, considering the influence of fluid flow. The WEBD simulation results demonstrate that such consideration is essential to describe the occurrence probability of long-length protrusions. Flow-regulated thermally nucleated protrusion theory is necessary to describe the unfolding behavior of collapsed polymer in low strain rate elongational flows. Neglecting the influence of flow results in significant overestimation of globular-stretch transition rate decrement with the strain rate. The transition from globular to stretched conformation at low elongation rates and long-length protrusion manifestation occurs on timescales potentially inaccessible to standard stochastic dynamic simulation. Thus, the verification of analytical results was not possible without the assistance of an enhanced sampling technique. Understanding the globular-stretch transition behavior of collapsed polymer under strain rate elongational flows below the critical value is relevant for analyzing the self-associated biopolymers response in the vicinity of blood vessel implant or design of flow responsive molecular structures for targeted drug therapy.

ACKNOWLEDGMENTS

The computational results presented have been achieved using the Extreme Science and Engineering Discovery Environment (XSEDE) [36], supported by the National Science Foundation, Grant No. ACI-1548562. Moreover, portions of this research were also conducted on Lehigh University's Research Computing infrastructure partially supported by the National Science Foundation Award No. 2019035. This work was supported in part by NSF Grant No. DMR-2004475 (to X.C. and X.F.Z.) and NIH Grants No. HL153986 and No. HL152348 (to X.F.Z.)

[1] F. Knoch and T. Speck, Phys. Rev. E **95**, 012503 (2017).
[2] H. Chen and A. Alexander-Katz, Phys. Rev. E **89**, 032602 (2014).
[3] C. Dong, S. Kania, M. Morabito, X. F. Zhang, W. Im, A. Oztekin, X. Cheng, and E. B. Webb, J. Chem. Phys. **151**, 124905 (2019).
[4] J. Jaspe and S. J. Hagen, Biophys. J. **91**, 3415 (2006).
[5] S. W. Schneider, S. Nuschele, A. Wixforth, C. Gorzelanny, A. Alexander-Katz, R. R. Netz, and M. F. Schneider, Proc. Natl. Acad. Sci. USA **104**, 7899 (2007).
[6] S. Goto, D. R. Salomon, Y. Ikeda, and Z. M. Ruggeri, J. Biol. Chem. **270**, 23352 (1995).
[7] M. Wittkop, S. Kreitmeier, and D. Göritz, Phys. Rev. E **53**, 838 (1996).
[8] R. G. Maurice and C. C. Matthai, Phys. Rev. E **60**, 3165 (1999).
[9] R. G. Larson, J. Rheol. **49**, 1 (2005).
[10] P. S. Doyle and E. S. G. Shaqfeh, J. Non-Newtonian Fluid Mech. **76**, 43 (1998).
[11] P. G. De Gennes, J. Chem. Phys. **60**, 5030 (1974).
[12] A. Alexander-Katz, H. Wada, and R. R. Netz, Phys. Rev. Lett. **103**, 028102 (2009).
[13] A. Halperin and E. B. Zhulina, Europhys. Lett. **15**, 417 (1991).
[14] A. Halperin and E. B. Zhulina, Macromolecules **24**, 5393 (1991).
[15] P. Y. Lai, Phys. Rev. E **53**, 3819 (1996).
[16] T. Frisch and A. Verga, Phys. Rev. E **65**, 041801 (2002).
[17] A. Alexander-Katz and R. R. Netz, Macromolecules **41**, 3363 (2008).
[18] A. Alexander-Katz, M. F. Schneider, S. W. Schneider, A. Wixforth, and R. R. Netz, Phys. Rev. Lett. **97**, 138101 (2006).
[19] C. E. Sing and A. Alexander-Katz, Macromolecules **43**, 3532 (2010).
[20] M. Radtke, S. Lippok, J. O. Rädler, and R. R. Netz, Eur. Phys. J. E **39**, 32 (2016).
[21] C. E. Sing and A. Alexander-Katz, J. Chem. Phys. **135**, 14902 (2011).
[22] A. H. Nguyen, S. Kania, X. Cheng, A. Oztekin, X. F. Zhang, and E. B. Webb, Macromolecules **54**, 8259 (2021).
[23] S. Kania, A. Oztekin, X. Cheng, X. F. Zhang, and E. Webb, Biophys. J. **120**, 1903 (2021).
[24] R. Schwarzl and R. R. Netz, Polymers **10**, 926 (2018).
[25] D. L. Ermak and J. A. McCammon, J. Chem. Phys. **69**, 1352 (1978).
[26] H. Yamakawa, J. Chem. Phys. **53**, 436 (1970).
[27] J. Rotne and S. Prager, J. Chem. Phys. **50**, 4831 (1969).
[28] G. A. Huber and S. Kim, Biophys. J. **70**, 97 (1996).
[29] B. W. Zhang, D. Jasnow, and D. M. Zuckerman, Proc. Natl. Acad. Sci. USA **104**, 18043 (2007).
[30] A. Nunes-Alves, D. M. Zuckerman, and G. M. Arantes, Biophys. J. **114**, 1058 (2018).
[31] D. M. Zuckerman and L. T. Chong, Annu. Rev. Biophys. **46**, 43 (2017).
[32] J. A. Kromer, L. Schimansky-Geier, and R. Toral, Phys. Rev. E **87**, 063311 (2013).
[33] D. Bhatt, B. W. Zhang, and D. M. Zuckerman, J. Chem. Phys. **133**, 14110 (2010).
[34] T. L. Hill, *Free Energy Transduction and Biochemical Cycle Kinetics* (Dover, New York, 1989).
[35] B. W. Zhang, D. Jasnow, and D. M. Zuckerman, J. Chem. Phys. **132**, 54107 (2010).
[36] J. Towns, T. Cockerill, M. Dahan, I. Foster, K. Gaither, A. Grimshaw, V. Hazlewood, S. Lathrop, D. Lifka, G. Peterson, R. Roskies, J. R. Scott, and N. Wilkins-Diehr, Comput. Sci. Eng. **16**, 62 (2014).